Journal of Al-Azhar University Engineering Sector

Vol.19 , No. 73, October 2024, 1239 - 1250

NONLINEAR COUPLING FACTOR MAXIMIZATION FOR A NEW CONFIGURATION OF ELECTROMAGNETIC ENERGY HARVESTER: NUMERICAL STUDIES AND SIMULATION

Mohammad Ahmad M. AbouTahoon*, Ramy Mohammed Elkady , Mohammad El-Faisal ElRifaie, Tarek Nasr Eldeen Mohammed

Mechanical Engineering Department, Faculty of Engineering, Al-Azhar University, Nasr City, 11884, Cairo, Egypt,

***Correspondence:** mohammadtahoon@azhar.edu.eg

Citation:

M. A. M. AbouTahoon, R.M. Elkady , M. E. ElRifaie, T. N. E. Mohammed, "Nonlinear Coupling Factor Maximization for A New Configuration Of Electromagnetic Energy Harvester: Numerical Studies And Simulation", Journal of Al-Azhar University Engineering Sector, vol. 19, pp.1239 -1250, 2024.

Received: 26 May 2024-05-

Revised: 02 July 2024

Accepted: 07 July 2024

DOI: 10.21608/auej.2024.292795.1670

ABSTRACT

Present paper explores a novel design of electromagnetic energy harvester to convert ambient vibration into electrical energy using induction. The emphasis of the current work is on the calculation of the nonlinear coupling factor of a novel architecture as well as comparing the system's response in either a linear or a nonlinear coupling, typically invoked and applied by the physics of the architecture. We hypothesize that considering the nonlinearities in coupling could be utilized to improve the output of the energy harvester by widening its frequency response. The design adopts two configurations, each is distinguished by the alignment direction of the easy magnetization axis with the direction of motion or normal to it, this approach shows high configurability of the system with low retrofitting effort. Our investigations showed that with such an architecture, the consideration of the nonlinear nature of the coupling is paramount to the tuning of the architecture to the amplitude of harvestable ambient vibrations.

KEYWORDS: Energy harvester, Mechanical Vibrations, Electromagnetic, nonlinear coupling

تعظيم عامل الاقتران غير الخطي لتكوين جديد لحصادة الطاقة الكهرومغناطيسية ـ دراسات عددية ومحاكاة

محمد أحمد محمد أبوطاحون*, رامى محمد القاضي , محمد الفيصل الرفاعى, طارق نصر الدين محمد

قسم الهندسة الميكانيكية، كلية الهندسة، جامعة الأزهر، مدينة نصر، 11884، القاهرة، مصر.

***البريد الاليكتروني للباحث الرئيسي:** mohammadtahoon@azhar.edu.eg

الملخص

تستكشف هذه الورقة استجابة محصد الطاقة الكهرومغناطيسية الذي يستخدم الحث لتحويل الاهتزاز المحيط إلى طاقة كهربائية. ينصب التركيز في العمل الحالي على مقارنة سلوك النظام في اقتران خطي أو غير خطي، والذي يتم استدعاؤه وتطبيقه عادةً

بواسطة فيزياء البنية. كانت فرضية هذه الدراسة هي أن الاقتران غير الخطي يستخدم لتحسين إنتاج محصد الطاقة من خلال توسيع الاستجابة الترددية. تبحث الدراسات التحليلية والعددية المجمعة في استجابة الحاصدة لكل من الإثارة الأساسية الفردية والمتعددة التردد. أظهرت تحقيقاتنا مناطق في الفضاء البارا متري حيث يكون الاقتران غير الخطي أفضل من الاقتران الخطي، والمناطق التي يكون العكس فيها صحيحًا. الاستنتاج المفيد هو أن الاقتران غير الخطي يمكن أن يكون ضارًا في بعض الأحيان، ولكنه قد يكون مفيدًا أيضًا إذا تم تنفيذه بشكل صحيح في النظام.

الكلمات المفتاحية: حاصد الطاقة، الاهتزازات الميكانيكية، الكهرومغناطيسية، اقتران غير خطى

1. INTRODUCTION

Micro-power generation is a rapidly developing area; the aim is to provide the power demands of wireless sensor networks and miniature electronic devices[1–4]. Electromagnetic energy harvesting is one of the main technologies for micro-power gleaning. It utilizes the rectilinear relative oscillation between a coil(s) and miniature magnet(s) to transduce mechanical energy to electrical energy through induction[5–7].

One of the promising application areas of micropower generation is in the field of Structural health monitoring (SHM), in this field the monitoring of the structural health depends on the autonomous detection of changes in the behavior of structures. Since localized damage in any structure large enough to reduce the stiffness; thus, increasing damping, should be detectable. The reduction in stiffness and/or increase in damping leads to a decrease in natural frequencies and consequently modify the vibration modes of the structure.

An effective detection and capture of such dynamic alterations is pertinent as a reliable method for the structural integrity quantification. However, a major requirement of sensor adaptation in existing technology is ability to power these SHM devices/sensors remotely and autonomously in a passive, efficient, ecofriendly way with minimum cost for retrofitting is. A device that could provide for power needs is a vibration energy harvester [8,9].

To optimize micropower generation systems and maximize the extraction of power with a specific set of design constrains, it is pertinent to accurately model and subsequently predict system behavior. The analysis paradigmatically proceeds from the first principles as follows: The basic vibration motion is modeled as a relative oscillation between one or more coils and a permanent magnet or magnets while the whole assembly is attached to a vibrating frame [5]. The damping in such models is attributed to two dissipation mechanisms, namely mechanical and electrical. The mechanical damping is almost exclusively modeled as viscous damping, and the electrical damping is solely due to the induced current in the coil; spurious eddy currents are typically neglected since the ambient vibrations are of low frequency [7], which is a reasonable assumption for most practical amplitudes and frequency ranges of covered vibrations, thus the electrical damping is proportional to velocity of the moving mass [10].

A unique feature of the present work is its emphasis on the investigation of nonlinear coupling in two novel configurations. The two configurations utilize different components of the magnetic field for electromagnetic coupling. The difference in the present configuration with respect to many configurations presented in literature[11], is the ability to change the orientation of the easy axes of magnetization with respect to direction of motion.

Typically the coupling models can be classified as: (i) a nonlinear coupling model, where the magnetic flux gradient depends on the position of coil relative to the magnet and (ii) a linear

coupling model, where the magnetic flux gradient has fixed value at all positions by virtue of being averaged over the coil area [4,5]. While the nonlinear model is considered more consistent with the physical system, the linear model is hypothetical and lends itself to easy optimization and direct calculation being formulated analytically in simple closed form. The specific nonlinear model of the present paper is detailed in later sections based on a novel architecture of magnet-coil interaction.

2. MATHEMATICAL MODEL

The first step to develop the model of the proposed configuration is to understand its Multiphysics from first principles. The following subsections develop an analytical model of the design, from system engineering point of view it is best to separate the device into its two subsystems: electromagnetic and mechanical, followed by the combined system equations. These equations then form the basis in the implementation of a numerical model of the harvester to parametrically design its components and to predict performance.

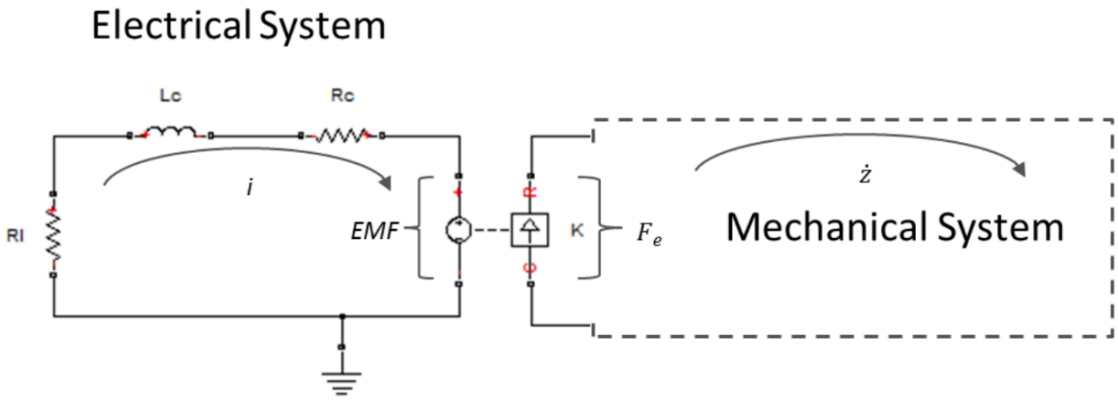

Figure 1: an abstract architecture of an EM energy harvester showing the importance of the coupling factor K.

The system engineering representation of a generic setup is shown in Figure 1. It consists of two subsystems; the mechanical subsystem is responsible for capturing the ambient vibrations through base excitation and transmitting it into the internal mass of the mechanical sub-system. The electrical subsystem is responsible for transducing the vibrational energy of the internal mass into electrical energy through induction and it should also include the lumped representation of the electrical component (parameters) of the system, to deliver the current into a rechargeable battery.

The mechanical subsystem in the proposed configuration is shown in Fig. 2 consisting of two rings to be made of a material that is transparent to magnetic field and acts as a frame to which four cubic magnets are fixed. The two rings with a fixed spacing construct the magnetic field. The cylindrical coil is rapped around a hollow rod as shown in upper right part of **Error! Reference source not found.**, the rod-coil assembly is free to move only axially within the frame assembly. A linear mechanical system is chosen which means the mechanical stiffness of the system is modeled as a linear spring and the mechanical damping are modeled as viscous damping only due the resistance to motion by the surrounding air, to keep the nonlinearities in the electrical system. Many previous studies have explored mechanical dynamical nonlinearities [7,14–17]. Note that the magnet assembly is fixed in place to the frame of reference (i.e. the vibrating structure), while the rod-coil assembly is allowed to vibrate in the z direction only and constrained radially. The electrical

subsystem Fig. 1 consists of the coil, with its associated inductance, internal resistance, coupling voltage, and a resistive load.

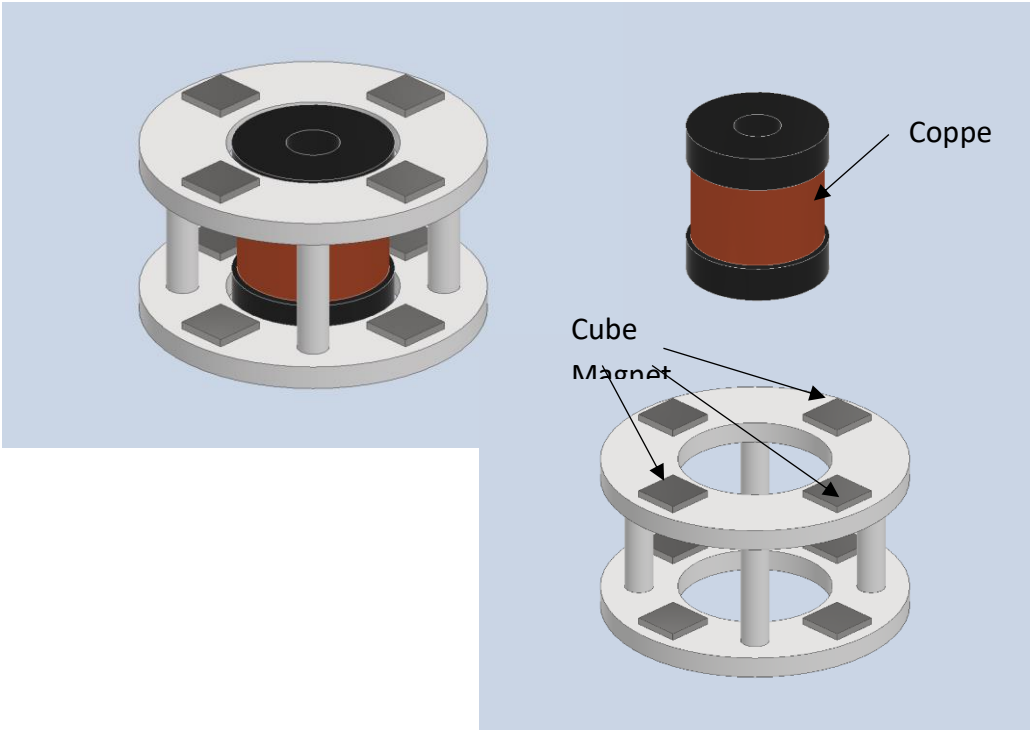

Figure 2: The new architecture of the electromagnetic energy harvester that is explored in the present work. The cube magnets are equally distributed in a circular ring of median diameter 24 mm. The spacing between the upper and lower rings are 20 mm.

2.1. PERMANENT CUBIC MANGNET

Permanent magnets are blocks of material directionally magnetized to act as pumps for magnetic field lines without external excitation by electric currents [18]. The flux density the magnets provide does not depend on their size, making it possible to use them where moderately high flux densities, on the order of one Tesla, are needed in very tight spaces [19].

Several types of permanent magnets exist, rare earth magnets often made of Samarium-Cobalt or Neodymium-Iron [20]. The production process consists of rapid cooling a molten mixture of the constituents, then crushing and/or grinding the mixture to a very fine powder. The powder is subjected to a strong magnetic field while under high pressure, this is intended to align the randomly oriented granular magnetic domains to their preferred crystallographic magnetic orientation. In a second step the blocks are pressed into shape and sintered, before being finished by machining to their final shape as blocks, cylinders, or disks. In the final stage, the material is exposed to an even higher magnetic field than the one they were subjected to in the first stage after rapid cooling. This process imprints the large remanent magnetic flux density B_r on the magnet, which can exceed 1 T for some materials. The direction in which the field is imprinted is usually termed the easy axis of the magnet [19].

The main characteristics of a magnet are summarized in the relation of a magnetic field H externally generated to the flux density B as

$$B_{\parallel} = \mu_r \mu_o H_{\parallel} + B_r \quad (1)$$

$$B_{\perp} = \mu_r \mu_o H_{\perp} \quad (2)$$

Where $B_{\parallel}$ is the flux density parallel to the easy axis and $B_{\perp}$ is the flux density normal to the flux density, while B_r is the remnant field imprinted by the magnetization process.

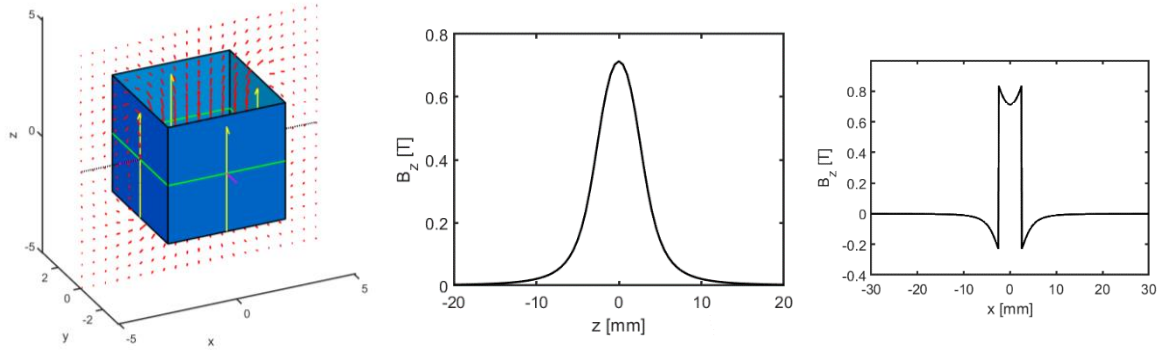

Figure 3: the current sheet idealization of the cubic magnet with length 5 mm and B_r=1.07 T, the coordinates origin at the center of the cube. The yellow arrow indicates the easy axis.

In the present work, we used the current sheet model of the permanent magnet [21]. The model used gives the magnetic field generated at a point located at position vector $\overrightarrow{r_2}$ by a plan sheet by the following equation:

$$\overrightarrow{\boldsymbol{B}}(\overrightarrow{r_2}) = \frac{B_r \alpha C}{4\pi}[(C-B)J_1 + BJ_3]\,(\overrightarrow{r_b} - \overrightarrow{r_a}) \times (\overrightarrow{r_2} - \overrightarrow{r_a}) + \frac{B_r \alpha C^2}{4\pi}[(C-B)J_2 - BJ_4]\vec{n} \quad (3)$$

Where the details of the method used to calculate the magnetic field is based on the integration of current sheets and the details of the calculations could be found in [22].

Figure 3 shows the magnetic field B_z or $B_{\parallel}$ for an equivalent current sheet model of a cubic magnet $5\ mm \times 5\ mm \times 5\ mm$, situated at the center of the coordinate system. On the left the change of the magnetic field at plane $y = 0$.

2.2. ELECTROMAGNETIC SUBSYSTEM

A generic electromagnetic vibration energy harvester benefits from Faraday's induction law (eq. 4): stating that the electromotive force (EMF) is equal to the time rate of change of total magnetic flux (ϕ) experienced by a nearby coil; to convert kinetic energy into electrical energy. The opposite polarity of the EMF induces a current, which in turn when closing the circuit invoke a magnetic force opposing the change in magnetic flux (Lenz' Law) thus the electrical damping.

The EMF is the difference in potential, or voltage, between the ends of the open-circuit coil. To embody Faraday's law in terms of coil parameters, the total magnetic flux equals the product of the total number of turns (N) and the average flux through each turn (ϕ), (eq. 5), the average flux is

computed as the surface integral of magnetic flux density (B) over the area (A) enclosed by the coil. The EMF will be therefore given by the flux spatial gradient multiplied by the velocity as in Equation 6. In the linear model of coupling, the average flux gradient of each turn is calculated as the product of the average flux density (B_{avg}) and the length of the wire in the coil (l_{wire}) to form Equation 7, where this product is termed the average electromechanical coupling coefficient (K).

$$EMF = -\frac{\mathrm{d}\Phi}{dt} \tag{4}$$

$$\Phi = N\phi = \sum_{i=1}^{N} \int_{A_i} B.dA \tag{5}$$

$$EMF = -N\frac{d\phi}{dz}\frac{dz}{dt} \tag{6}$$

$$EMF = -N\, c_f\, B_{avg} l_{wire} \dot{z} = -K\, \dot{z} \tag{7}$$

Equation 7 is the typical linear model definition of the coupling factor K in which N_f is the coil fill factor i.e. the percentage of the coil geometrical cross-sectional area occupied by the copper wire, and l_{wire} is the effective length of the coil. For a specific coil design, the coupling equation fixes three coil parameters, namely the number of turns, the length, and the fill factor, while the parameter B_{avg} despite being a variable in real application is averaged out [22,23]. The coil three parameters are considered fixed because it is specific to the design meaning that once the coil has been fabricated, those values cannot be altered. The linear model is justifiable if the configuration of the harvester is simple (single cylindrical magnet, that could be modeled as magnetic dipole), and the distance between the magnet and the coil are in the order of magnitude of the magnet radius.

However, for the proposed configurations in the present paper, it was necessary to consider the coupling in more detail and that leads to the determination of the coupling factor (K) as a nonlinear function of the relative displacement between the coil and the magnets.

To complete the description of the electromagnetic subsystem, using Kirchhoff's Voltage law, to calculate the potential difference between the two terminals in fig. 1 as given by eq. 8, where R_c, is coil resistance, L_c, coil inductance and R_l, load resistance. Then the current induced i in the closed circuit is solved for as in eq. 9.

$$-K\dot{z} + i\,(R_l + R_c + j\omega L_c) = 0 \tag{8}$$

$$i = \frac{K\dot{z}}{R_l + R_c + j\omega L_c} \tag{9}$$

The magnetic force (Lorenz force) this current creates, given by Equation 10, acts as to oppose the translation motion of the coil through the magnetic field. Lorenz force is manifested mechanically as a viscous damping force (i.e. function of the velocity) and can be expressed mathematically in an analogous way to mechanical viscous damping by an electric damping coefficient c_e, as given by eq. 11.

$$F_e = Ki = c_e\dot{z} \tag{10}$$

$$c_e = \frac{K^2}{R_l + R_c + j\omega L_c} \tag{11}$$

Moreover, as can be seen, the coupling factor plays the dominant role in determining the electrical damping as well as the extractable power from the harvester when there is a load, i.e. battery charging.

The total electrical power P_e in the coil-load circuit is driven by this damping action, eq. 12, where the amount extracted by the load could be represented by the load electric damping coefficient C_e^l, as in eq. 13, while the remaining portion is dissipated as heat by C_e^d, defined in eq. 14.

$$P_e = \frac{EMF^2}{R_l + R_c + j\omega L_c} = c_e \dot{z}^2 \tag{12}$$

$$P_e^{load} = \frac{R_l}{R_l + R_c + j\omega L_c} P_e = C_e^l \dot{z}^2 \tag{13}$$

$$P_e^{dissipated} = \frac{R_c}{R_l + R_c + j\omega L_c} P_e = C_e^d \dot{z}^2 \tag{14}$$

2.3. THE PROPOSED CONFIGURATION

In this section, an explanation of the novel configuration that we are proposing. As shown in Figure 4**Error! Reference source not found.**, the proposed configuration is composed of two sets of 4 cubic magnets each, the first set of four magnets are arranged equally spaced on the circumference of a circle in the same plane. While the other set is offset by a spacing 20 mm to the south of the first set, such that the coordinate system's origin lies at the two rings' midplane.

In configuration one all the magnets' easy axes are aligned parallel to the $z - axis$, the axis of motion of the coil. While the configuration two shown in Figure 5, the alignment of the magnets' easy axes is normal to the direction of the $z - axis$, the direction of the coil motion, this configuration was inspired by axial field machines design.

In both configurations, the coil is situated initially at the center of the midplane between the upper and lower rings, while the outer diameter of the coil was never to exceed the internal diameter of the magnet ring. This configuration was hypothesized to enable maximizing the axial flux utilization for the transduction.

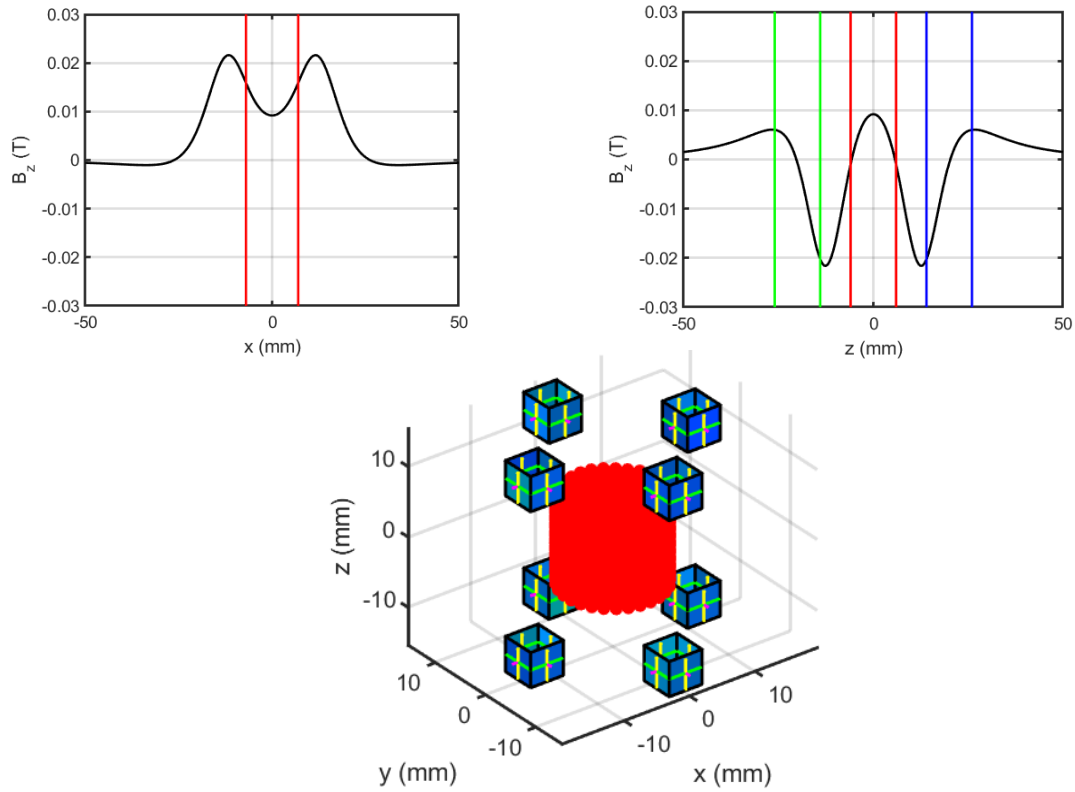

Figure 4: Configuration one, showing four cubic magnets (5 mm in size) radial aligned in a ring with radius 10 mm, and the spacing between the upper and the lower ring is 20 mm. The location of the induction coil is shown in red, and initially located at the center of the coordinate system. The coil has inner radius of 2 mm and outer radius of 4 mm, and height of 12 mm. In this configuration all the magnets' easy axis are aligned in the z direction as illustrated by the yellow arrows.

2.4. DETAILED CALCULATION OF THE COUPLING FACTOR

To find the resulting EMF from the configuration presented earlier, an analytical expression of the magnetic flux of a single coil will be first derived. Magnetic flux, a measure of the magnetic field over an area, is given by the dot product of $\vec{\boldsymbol{B}}$ and that area, i.e. $\Phi = \oint_S \boldsymbol{B}.d\boldsymbol{A}$, where S is the surface of the area thus $d\boldsymbol{A}$ is infinitesimal slice of this surface. Using the B-field expression given in eq. 3 and using as the surface the circle enclosed by a single turn of the coil, the flux becomes:

$$\Phi = \int_0^{2\pi} \int_0^{r} \boldsymbol{B}.\hat{k}(r\, dr\, d\phi) \tag{15}$$

For the proposed architecture, it is important to obtain the average flux over the entire length and width of the finite coil. Integrating over the length and width gives the sought after average flux expression for all coil turns over its cross-section.

$$\Psi = \frac{1}{A_c} \int_{z_l}^{z_u} \int_{r_i}^{r_o} \Phi\, dr\, dx \tag{16}$$

The integrations in the present work were carried out numerically using the Simpson 1/3 rule, as shown by the MATLAB code in the appendix.

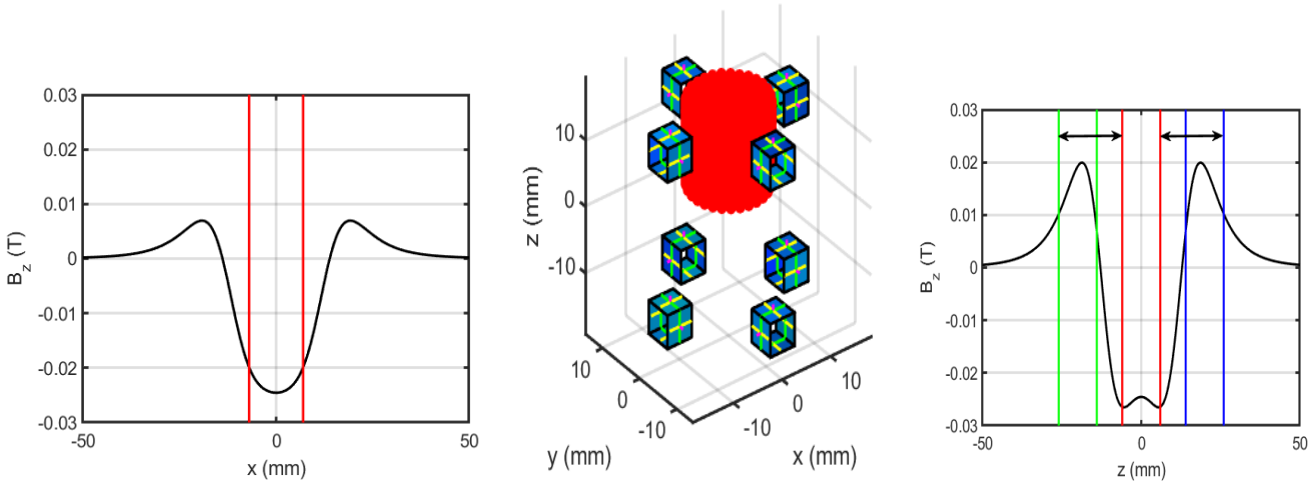

Figure 5: Configuration two, showing four cubic magnets (5 mm in size) radial aligned in a ring with radius 10 mm, and the spacing between the upper and the lower ring is 20 mm. The location of the induction coil is shown in red, and initially located at the center of the coordinate system. The coil has inner radius of 2 mm and outer radius of 4 mm, and height of 12 mm. In this configuration all the magnets' easy axis are aligned normal

3. RESULTS AND DISCUSSION

The coupling factor calculations for configuration one done numerically is shown in Figure 6, the alignment of the coil with easy axis of the magnet enables a high coupling for relatively small motions around the null position $(z = 0)$ thus maximizing the energy conversion with small amplitudes. While in configuration two shown in Figure 7, illustrates a high negative coupling factor that could overcome a high electrical damping, making the axial flow design more robust for high amplitude vibrations.

4. CONCLUSIONS

Two configurations of an electromagnetic harvester using cubical magnets and toroidal coil geometries was analyzed. In the first configuration of the coil were allowed to oscillate

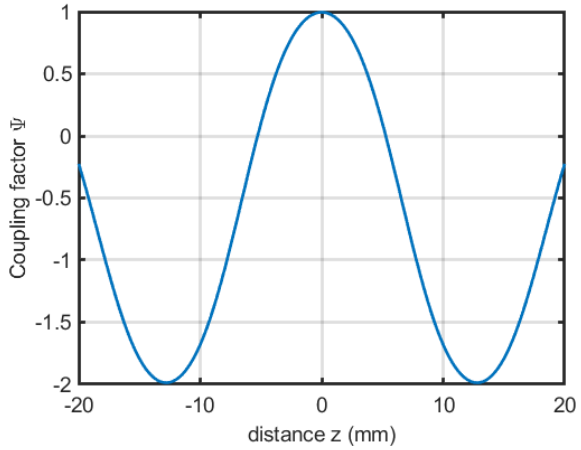

Figure 6: The non-normalized coupling factor of configuration one. As function of relative distance d between the center of the coil and the center between the upper and lower magnet rings.

perpendicular to the easy axis of the magnet, it is shown that the instantaneous definition of the coupling factor is appropriate as means of quantifying the electrical damping in a nonlinear manner. It was further shown that for small oscillations, the alignment of the moving coil in the same direction of the easy axis is conducing to an almost constant coupling factor with high value.

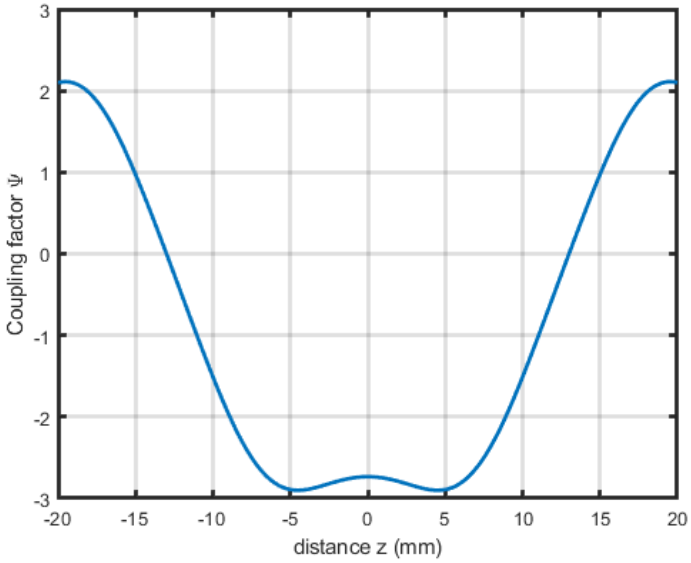

Figure 7: The non-normalized coupling factor of configuration Two. As function of relative distance d between the center of the coil and the center between the upper and lower magnet rings

APPENDIX: MATLAB Code

```
N_r = 20;
N_theta = 20;
d_coil = 0.25;
r_i = 4;
r_o = 8;
coil_half = 6;

rr = r_i:d_coil:r_o;
zz = -coil_half+delta:d_coil:coil_half+delta;
theta = linspace(0,2*pi,N_theta);
I_zz = 0.*zz;

parfor k=1:length(zz)
   Icoil = 0.*rr; % for parallel
   for irr = 1:length(rr)
      r = linspace(0,rr(irr), N_r);
   % loop over theta
   I = 0.*theta; %for parallel
      for ii = 1:length(theta)
   % integration over radius
         B = BZRT(theta(ii), r, zz(k), sheets);
         temp = r.*B;
         oddi = 3:2:length(r)-1;
         Odd = sum(temp(oddi), 'omitnan');
         eveni = 2:2:length(r)-2;
         Even = sum(temp(eveni), 'omitnan');
         I(ii) = (abs(r(2)-r(1))/3)*(temp(1)+temp(end)+4*Odd+2*Even);
```

```
    end

  % using Simpsons 1/3 Rule
  OddIndex = 3:2:length(theta)-1;
  EvenIndex =2:2:length(theta)-1;
  Icoil(irr) = (abs(theta(2)-theta(1))/3)*(I(1)+I(end)+ 4*sum(I(OddIndex), 'omitnan')+2*sum(I(EvenIndex), 'omitnan'));
  end
  Od = 3:2:length(Icoil)-1;
  ev = 2:2:length(Icoil)-1;
  I_rr= (d_coil/3)*sum([Icoil(1), Icoil(end), 2*sum(Icoil(ev), 'omitnan'), 4*sum(Icoil(Od), 'omitnan')], 'omitnan');
  I_zz(k)= I_rr;
end
oo = 3:2:length(I_zz)-1;
ee = 2:2:length(I_zz)-1;
out = (d_coil/3)*sum([I_zz(1), I_zz(end), 2*sum(I_zz(ee), 'omitnan'), 4*sum(I_zz(oo), 'omitnan')], 'omitnan');
a_c = (r_o -r_i)*2*coil_half;
out = out/a_c;
```

References

[1] Amirtharajah R, Chandrakasan AP. Self-powered signal processing using vibration-based power generation. IEEE J Solid-State Circuits 1998;33:687–95. https://doi.org/10.1109/4.668982.

[2] Bedekar V, Oliver J, Priya S. Pen harvester for powering a pulse rate sensor. J Phys D: Appl Phys 2009;42:105105. https://doi.org/10.1088/0022-3727/42/10/105105.

[3] Izhar, Khan FU. Electromagnetic based acoustic energy harvester for low power wireless autonomous sensor applications. SR 2018;38:298–310. https://doi.org/10.1108/SR-04-2017-0062.

[4] Sasaki K, Osaki Y, Okazaki J, Hosaka H, Itao K. Vibration-based automatic power-generation system. Microsyst Technol 2005;11:965–9. https://doi.org/10.1007/s00542-005-0506-8.

[5] Holm P, Imbaquingo C, Mann BP, Bjørk R. High power electromagnetic vibration harvesting using a magnetic dumbbell structure. Journal of Sound and Vibration 2023;546:117446. https://doi.org/10.1016/j.jsv.2022.117446.

[6] Ahmad MM, Khan FU. Review of vibration-based electromagnetic–piezoelectric hybrid energy harvesters. International Journal of Energy Research 2021;45:5058–97. https://doi.org/10.1002/er.6253.

[7] Carneiro P, Soares Dos Santos MP, Rodrigues A, Ferreira JAF, Simões JAO, Marques AT, et al. Electromagnetic energy harvesting using magnetic levitation architectures: A review. Applied Energy 2020;260:114191. https://doi.org/10.1016/j.apenergy.2019.114191.

[8] Cepnik C, Radler O, Rosenbaum S, Ströhla T, Wallrabe U. Effective optimization of electromagnetic energy harvesters through direct computation of the electromagnetic coupling. Sensors and Actuators A: Physical 2011;167:416–21. https://doi.org/10.1016/j.sna.2011.01.023.

[9] Toluwaloju TI, Thein CK, Halim D. An Effect of Coupling Factor on the Power Output for Electromagnetic Vibration Energy Harvester. The 8th International Electronic Conference on Sensors and Applications, MDPI; 2021, p. 5. https://doi.org/10.3390/ecsa-8-11279.

[10] Tong W. Mechanical Design and Manufacturing of Electric Motors. 2nd ed. Boca Raton: CRC Press; 2022. https://doi.org/10.1201/9781003097716.

[11] Harb A. Energy harvesting: State-of-the-art. Renewable Energy 2011;36:2641–54. https://doi.org/10.1016/j.renene.2010.06.014.

[12] Shan X, Xu Z, Xie T. New Electromechanical Coupling Model and Optimization of an Electromagnetic Energy Harvester. Ferroelectrics 2013;450:66–73. https://doi.org/10.1080/00150193.2013.838491.

[13] Cannarella J, Selvaggi J, Salon S, Tichy J, Borca-Tasciuc D-A. Coupling Factor Between the Magnetic and Mechanical Energy Domains in Electromagnetic Power Harvesting Applications. IEEE Trans Magn 2011;47:2076–80. https://doi.org/10.1109/TMAG.2011.2122265.
[14] Dallago E, Marchesi M, Venchi G. Analytical Model of a Vibrating Electromagnetic Harvester Considering Nonlinear Effects. IEEE Trans Power Electron 2010;25:1989–97. https://doi.org/10.1109/TPEL.2010.2044893.
[15] Firoozy P, Friswell MI, Gao Q. Using time delay in the nonlinear oscillations of magnetic levitation for simultaneous energy harvesting and vibration suppression. International Journal of Mechanical Sciences 2019;163:105098. https://doi.org/10.1016/j.ijmecsci.2019.105098.
[16] Apo DJ, Priya S. High Power Density Levitation-Induced Vibration Energy Harvester. Energy Harvesting and Systems 2014;1:79–88. https://doi.org/10.1515/ehs-2013-0005.
[17] Xu J, Leng Y, Sun F, Su X, Chen X. Modeling and performance evaluation of a bi-stable electromagnetic energy harvester with tri-magnet levitation structure. Sensors and Actuators A: Physical 2022;346:113828. https://doi.org/10.1016/j.sna.2022.113828.
[18] Roy SB. Experimental Techniques in Magnetism and Magnetic Materials n.d.
[19] Coey JMD, Parkin SSP, editors. Handbook of Magnetism and Magnetic Materials. Cham: Springer International Publishing; 2021. https://doi.org/10.1007/978-3-030-63210-6.
[20] Mikolanda T, Košek M, Richter A. Magnetic Field of permanent magnets: Measurment, Modelling, Visualization n.d.
[21] Ziemann V. Hands-on accelerator physics using MATLAB®. Boca Raton, FL: CRC Press, Taylor & Francis Group; 2019. https://doi.org/10.1201/9780429491290.
[22] Furlani EP. Permanent magnet and electromechanical devices: materials, analysis, and applications. San Diego, Calif: Academic; 2001.
[23] Ravaud R, Lemarquand G. COMPARISON OF THE COULOMBIAN AND AMPERIAN CURRENT MODELS FOR CALCULATING THE MAGNETIC FIELD PRODUCED BY RADIALLY MAGNETIZED ARC-SHAPED PERMANENT MAGNETS. PIER 2009;95:309–27. https://doi.org/10.2528/PIER09042105.